ELSEVIER

Journal of Organometallic Chemistry 569 (1998) 159–167

Journal of Organometallic Chemistry

Ethylene polymerization catalysts based on nickel(II) 1,4-diazadiene complexes: the influence of the 1,4-diazadiene backbone substituents on structure and reactivity[1]

Thomas Schleis [a], Thomas P. Spaniol [a], Jun Okuda [a,*], Johannes Heinemann [b], Rolf Mülhaupt [b]

[a] *Institut für Anorganische Chemie und Analytische Chemie, Johannes Gutenberg-Universität Mainz, J.-J.-Becher-Weg 24, D-55099 Mainz, Germany*

[b] *Freiburger Materialforschungszentrum und Institut für Makromolekulare Chemie, Albert-Ludwig-Universität Freiburg, Stefan-Meier-Strasse 21, D-79104 Freiburg, Germany*

Received 1 April 1998

Abstract

Thermally sensitive dialkyl nickel complexes {DAD(H,H)}Ni(CH_2SiMe_3)$_2$ and {DAD(Me,Me)}Ni(CH_2SiMe_3)$_2$ [DAD(X,X) = 2,6-*i*Pr$_2$C$_6$H$_4$–N=C(X)–C(X)=N–C$_6$H$_4$*i*Pr$_2$-2,6] were synthesized and were characterized by X-ray diffraction studies on single crystals. The substituents X on the backbone of the α-diimine ligand significantly influence the conformation of the 2,6-diisopropylphenyl substituents. This effect is thought to be of crucial importance for the polymerization of ethylene when {DAD(X,X)}NiBr$_2$/MAO is used as catalyst. The influence of the catalyst structure, pressure, and temperature on the polymerization activity, molar mass, glass transition temperature, melting temperature and branching of the polymers has been studied. The dialkyl complex {DAD(H,H)}Ni(CH_2SiMe_3)$_2$ underwent rapid reductive carbonylation giving the dicarbonyl complex {DAD(H,H)}Ni(CO)$_2$ along with both bis(trimethylsilyl)ethane and α,α′-bis(trimethylsilyl)acetone. The dicarbonyl {DAD(H,H)}Ni(CO)$_2$ was characterized by X-ray crystallography.

Keywords: X-ray crystallography; Polymerization catalyst; 1,4-Diazadiene ligand; Nickel alkyl complexes; Reductive carbonylation

1. Introduction

In the mid 1980s homogeneous nickel catalysts [1] for the oligo- and polymerization of ethylene to produce short-chain branched polyethylene became available [2]. The basis for an unprecedented type of polymerization was the discovery of the so-called 2,ω-polymerization by Fink et al. [3]. Using nickel(0) catalysts, α-olefins such as 1-pentene do not form poly(α-olefin) as would be expected with Ziegler-type catalysts, but instead gives polyethylene with methyl branches corresponding to poly(ethylene-*alt*-propylene). More recently, Brookhart et al. ([4]c) introduced highly efficient nickel and palladium catalysts for the synthesis of branched polyethylenes [4]. They are based on substituted 1,4-diazadiene or α-diimine ligands containing sterically bulky 2,6-diisopropylphenyl substituents at the imine nitrogen atoms: 2,6-*i*Pr$_2$C$_6$H$_4$–N=C(X)–C(X)=N–C$_6$H$_4$*i*Pr$_2$-2,6 [DAD(X,X): X = H, Me; X$_2$ = acenaphtylene]. This type of ligand has long been known, e.g. as ancillary ligands for group 10 metal catalysts for the oligomerization of alkynes [5–7]. It was noted [4] that the presence of the 2,6-diisopropylphenyl substituents is of critical importance in generating a suitable coordination sphere at the cationic nickel(II) center. The branching was attributed to the migration of the nickel alkyl along the polymer chain through repetitive β-H elimination and reinsertion of the vinyl-

* Corresponding author. Fax: +49 6131 395605.

[1] Dedicated to Professor Akira Nakamura with best personal wishes.

0022-328X/98/$19.00
PII S0022-328X(98)00784-0

terminated polymer into the metal-hydride bond. We report here the synthesis and X-ray diffraction studies of two nickel dialkyls containing 1,4-diazadiene ligands derived from glyoxal and diacetyl. Trimethylsilymethyl was used for the alkyl groups on the nickel center, since it gives thermally more stable nickel derivatives and it has been proven to be a useful model for a growing polymer chain [8]. We also present detailed data on the ethylene polymerization behavior of nickel catalysts based on the DAD(X,X) ligands.

2. Results and discussion

Easily accessible, paramagnetic dibromo complexes {DAD(H,H)}$NiBr_2$ (**1**) and {DAD(Me,Me)}$NiBr_2$ (**2**) [6] can be activated by methylalumoxane (MAO) to give the cationic species [{DAD(X,X)}NiMe]$^+$ [MAO]$^-$ active for the polymerization of olefins [4]. The generation of [{DAD(H,H)}NiMe]$^+$[B{C_6H_3-$(CF_3)_2$-3,5}$_4$]$^-$ was reported by Brookhart et al. ([4]c) but its isolation was hampered by extreme temperature-sensitivity. We found that even the dimethyl precursor {DAD(X,X)}$NiMe_2$, previously reported in the literature [6] was difficult to handle. When **1** and **2** are treated with the Grignard reagent $Mg(CH_2SiMe_3)Cl$ in ether at -78°C, the new dialkyl complexes {DAD(H,H)}$Ni(CH_2SiMe_3)_2$ (**3**) and {DAD(Me,Me)}-$Ni(CH_2SiMe_3)_2$ (**4**) are isolated in analytically pure form in 18 and 28% yield, respectively (Scheme 1). The turquoise extremely air- and moisture-sensitive crystals are stable at 25°C. However, both compounds rapidly decompose in solution above 0°C and substantial care must be taken for their isolation to be successful.

According to ^{1}H- and ^{13}C-NMR spectra, compounds **3** and **4** have apparent C_{2v}-symmetry in solution. The two separated doublets for the four isopropyl groups of the aromatic ring indicate both hindered rotation about the nitrogen *ipso* carbon and the isopropyl *ortho* carbon bond. The trimethylsilymethyl groups in **3** give rise to two signals at δ 0.08 and 2.32 in the ratio 2:9. The corresponding signals of **4** appear at 0.05 and 1.17. In **3** the methylene protons are recorded at 25°C as a broad signal, indicating fluxional behavior. If the C_2-symmetric structure found in the crystal lattice reflects the preferred conformation, the methylene protons are diastereotopic. It is noteworthy that the methyl groups of the 1,4-diazadiene backbone in **4** have undergone a high-field shift of almost 2 ppm upon complexation, indicating their close proximity to the aromatic imine substituents. Reaction of the dialkyl complexes with the strong Brønsted acid H(Et_2O)[B{$C_6H_3(CF_3)_2$-3,5}$_4$] led to decomposition, resulting in intractable product mixtures.

In order to explore the nature of the nickel-carbon bond in the dialkyl **3**, carbonylation was studied. When a hexane solution of the dialkyl **3** at 25°C is exposed to slight excess of CO at 1 bar, followed by partial evaporation of solvent and crystallization at –30°C, the dicarbonyl {DAD(H,H)}$Ni(CO)_2$ (**5**) can be isolated as red crystals. The CO ligands give rise to a ^{13}C-NMR resonance at 196.9 ppm and two ν_{CO} bands in the IR spectrum at 2014 and 1954 cm^{-1}. The carbonylation of **3** to give **5** is accompanied by the formation of the organic byproducts $Me_3SiCH_2CH_2SiMe_3$ (**6**) and $(Me_3SiCH_2)_2CO$ (**7**). It can be regarded as a reductive elimination, preceded by CO insertion into the nickel–alkyl bond. This type of reaction has been studied extensively by Yamamoto et al. ([9]a) using dialkyl complexes of the type L_2NiR_2, where L are two-electron donor, and R are alkyl ligands [9]. These authors observed the formation of the alkane R-R, ketone R-CO-R, diketone R-CO–CO-R, and aldehyde R-CHO as products of reductive elimination depending on the complex used and the reaction conditions. When **3** is reacted with slight excess of CO at r.t. in benzene-d_6, the reaction mixture clearly contains both the alkane **6** and the ketone **7**. In dichloromethane, the reaction of **3** at -60°C with a slight excess of CO gave

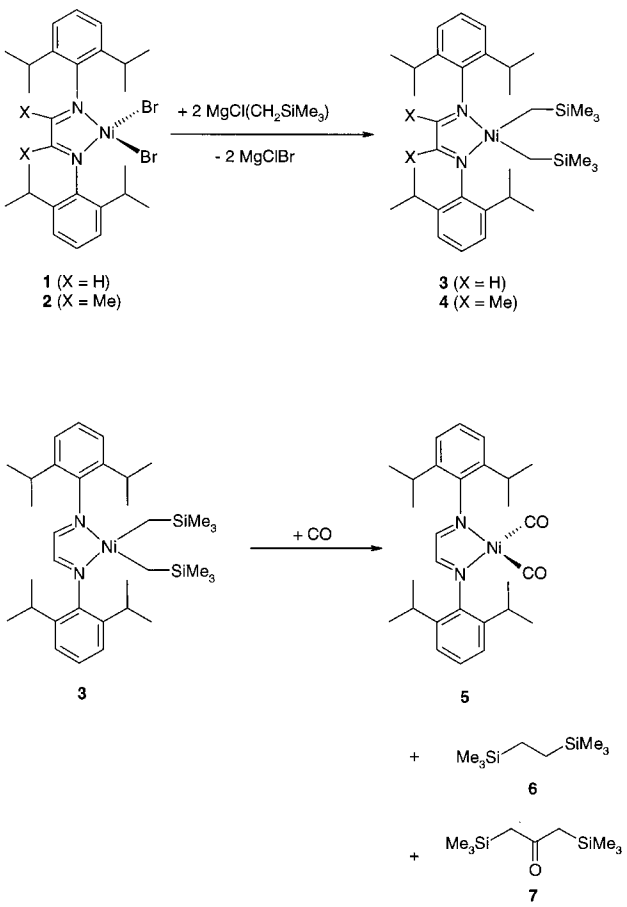

Scheme 1.

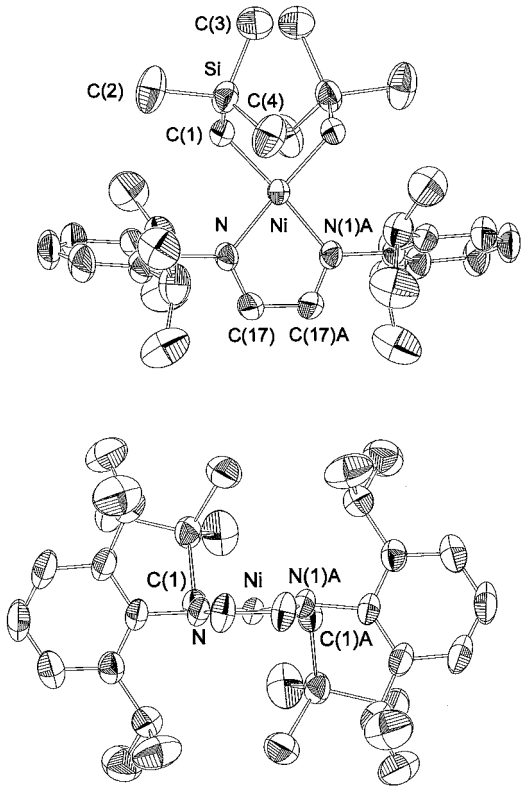

Fig. 1. ORTEP diagrams for the molecular structure of {DAD(H,H)}Ni(CH_2SiMe_3)$_2$ (**3**). Thermal ellipsoids are drawn at the 50% probability level. Hydrogen atoms have been omitted for the sake of clarity.

only the ketone **7**, with the dicarbonyl complex **5** decomposing at -20°C.

2.1. Crystal structures

Despite their pronounced sensitivity, single crystals of the dialkyl complexes **3** and **4** could be obtained and analyzed by X-ray diffraction. Figs. 1 and 2 show the ORTEP-plots of the compounds **3** and **4**. Selected bond lengths and angles are listed in Table 1.

The overall molecular structure of both compounds can be described as square planar, typical for a d^8 nickel(II) center with strong ligands. Both compounds reside on a crystallographic C_2-axis with the two bulky trimethylsilyl groups arranged on opposite sides of the planar Ni{DAD(X,X)} fragment. Upon closer inspection, however, the conformation of the ligand periphery is different for the two compounds. The ORTEP plot of **3** shows how the isopropyl groups of the 2,6-diisopropylphenyl substituent are tilted away from the nickel center. This effect can be explained by steric repulsion of the bulky alkyl substituents. In **4** on the other hand, the isopropyl groups are turned towards the nickel dialkyl unit. This reduction of the space at the nickel center is evidently caused by the two methyl groups of the 1,4-diazadiene backbone. The angle between the mean plane defined by the aromatic ring and the mean plane defined by the atoms N, N(1)A, C(17), C(17)A, and Ni is 76.6° for **3** and 83.4° for **4**. This shows that in the latter complex, the aromatic ring is less tilted towards the diazadiene backbone.

For the polymerization of olefins it seems to be important that the aromatic residues at the 1,4-diazadiene bridge have bulky substituents in the *ortho*-positions. Brookhart and coworkers [4] showed that compounds with methyl substituents give lower molecular weight and unbranched polyolefins. Isopropyl substituents increase the molecular weight and allow isomerization and 'chain walking' to take place. It is therefore important to understand the influence of the isopropyl groups. Its steric bulk blocks the chain termination step and allows isomerization to take place. The available space at the nickel center is the key to the control of the polymerization behavior. The free space at the metal center is partly controlled by non-bonded interaction to the methyl groups of the isopropyl units. The molecular structures show that the shortest distances are 4.550(5) and 5.120(3) Å for **3** compared to 4.424(4) and 5.029(4) Å for **4**. In addition, the distances between the same methyl groups and C(1) are 5.066(4) and 4.846 (4) Å in **3** compared to 4.071(4) and 4.624(5)

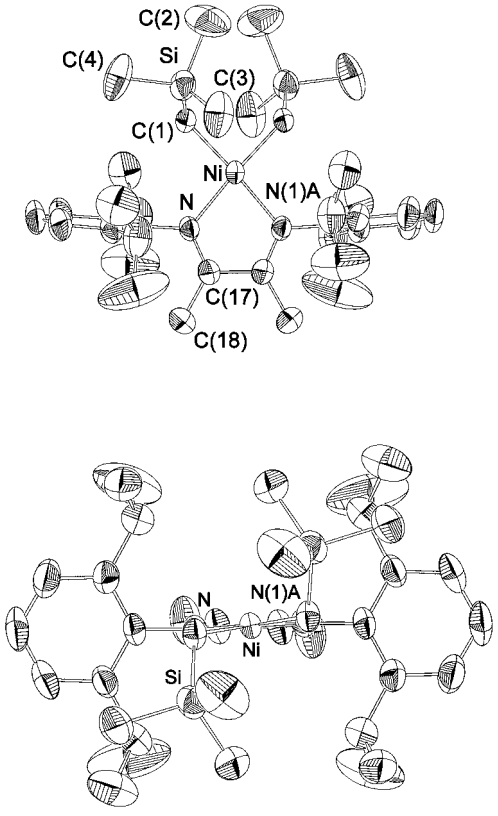

Fig. 2. ORTEP diagrams for the molecular structure of {DAD(Me,Me)}Ni(CH_2SiMe_3)$_2$ (**4**). Thermal ellipsoids are drawn at the 50% probability level. Hydrogen atoms have been omitted for the sake of clarity.

Table 1
Selected bond lengths (Å) and angles (°) of {DAD(H,H)}Ni-$(CH_2SiMe_3)_2$ (**3**) and {DAD(Me,Me)}Ni$(CH_2SiMe_3)_2$ (**4**)

	3 (X = H)	**4** (X = Me)
Ni–C(1)	1.950(2)	1.955(2)
Ni–N	1.964(1)	1.974(2)
N–C(17)	1.293(2)	1.294(3)
N–C(5)	1.449(2)	1.445(3)
C(10)–C(14)	1.512(3)	1.513(4)
C(11)–C(12)	1.517(4)	1.499(4)
C(11)–C(13)	1.528(4)	1.516(5)
C(14)–C(16)	1.529(5)	1.502(7)
C(14)–C(15)	1.538(4)	1.531(5)
C(17)–C(17)A	1.432(4)	1.471(5)
C(1)–Ni–C(1)A	88.0(1)	87.9(1)
C(1)–Ni–N(1)A	174.84(7)	174.45(9)
C(1)A–Ni–N(1)A	95.71(1)	96.34(8)
N(1)A–Ni–N	80.78(9)	79.6(1)
C(17)–N–Ni	114.1(1)	115.9(2)
Si–C(1)–Ni	116.1(1)	119.4(1)
N–C(17)–C(17)A	115.5(1)	114.0(1)

Thermal ellipsoids are drawn at 50% probability level.

Å in **4**. This shows that the isopropyl methyl groups are closer to the central metal atom in **4** than in **3**. We anticipate that the catalytically active species derived from the closely analogous precursors **1** and **2** should also provide more space for polymerization reactions in the former.

For both structures the angle C(1)–Ni–C(1)A of 88° is the same, within the standard deviation, but the angle at the methylene carbon Si–C(1)–Ni in **4** is larger by 3°. Thus, the trimethylsilyl groups of **4** are forced away further from the nickel center than those in **3**. Interestingly the carbon–carbon bond lengths C(17)–C(17)A differ quite substantially, with 1.432(4) Å for **3** and 1.471 (5) Å for **4**. The larger bond length in **4** seems to reflect the electronic and steric effects of the two additional methyl groups at the 1,4-diazadiene bridge. This difference can also be seen in the angles at the imine nitrogen atom and nickel atom C(17)–N–Ni and N–Ni–N(1)A.

There are no published crystal structure analyses of dialkyl nickel complexes with sterically hindered 1,4-diazadienes, but the molecular structure of a bis(trimethylsilylmethyl) complex, $py_2Ni(CH_2SiMe_3)_2$, has been described [10]. The nickel atom finds itself in a nearly perfect square planar, unconstrained coordination sphere with values of the angles at the metal N–Ni–C(1) of 92.5° and N–Ni–N(1) of 87.5°.

The crystal structure analysis of the dicarbonyl compound **5** could also be established. Fig. 3 depicts the ORTEP diagram of the dicarbonyl **5**. Selected bond lengths and angles are listed in Table 2. The molecular structure of **5** shows a distorted tetrahedral geometry,

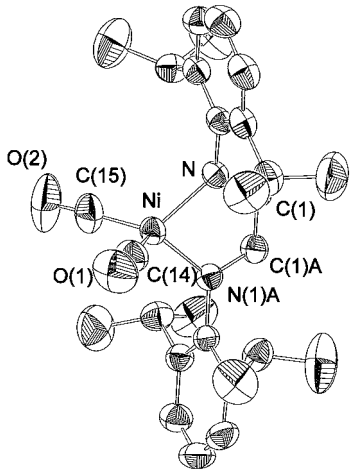

Fig. 3. ORTEP diagrams for the molecular structure of {DAD(H,H)}Ni$(CO)_2$ (**5**). Thermal ellipsoids are drawn at the 50% probability level. Hydrogen atoms have been omitted for the sake of clarity.

as generally expected for zero-valent dicarbonyl nickel complexes. For instance, it is similar to the structure of (dicarbonyl)(4,6-dimethyl-2,2′-bipyridyl)nickel [11]. The nickel–imine nitrogen distances are slightly longer than those in **3**, which can be explained by the presence of the strong π-acceptor ligand CO at the nickel center. The angle N–Ni–N(1)A of 80.3(1)° can be regarded as a consequence of the chelating 1,4-diazadiene ligand, distorting the idealized tetrahedral configuration of the nickel.

2.2. Polymerizations

Polymerizations of α-olefins using MAO-activated catalysts {DAD(H,H)}$NiBr_2$ (**1**) and {DAD(H,H)}-$NiBr_2$ (**2**) have been reported by Brookhart et al. [4] to give polymers with a randomly distributed multiply branched structure, with predominantly methyl

Table 2
Selected bond lengths (Å) and angles (°) of {DAD(H,H)}Ni$(CO)_2$ (**5**)

Ni–C(15)	1.756(5)
Ni–C(14)	1.761(4)
Ni–N	1.971(2)
N–C(1)	1.291(3)
N–C(2)	1.444(3)
O(1)–C(14)	1.135(5)
O(2)–C(15)	1.134(5)
C(15)–Ni–C(14)	105.6(2)
C(15)–Ni–N	117.6(1)
C(14)–Ni–N	117.4(1)
N–Ni–N(1)A	80.3(1)
C(1)–N–C(2)	119.5(2)
C(1)–N–Ni	113.8(2)
C(2)–N–Ni	126.5(2)
N–C(1)–C(1)A	115.8(1)

Table 3
Ethylene polymerization data using MAO-activated **1** and **2**

Run	Catalyst precursor[a]	P^b (bar)	f_E^c (mol l^{-1})	T_P^d (°C)	A^e (kg ($mol_{Ni} \cdot h \cdot mol\ l^{-1})^{-1}$)	M_n^f (g mol^{-1})	T_m^g (°C)	N^h
1	1	1.5	0.22	20	2700	56 300	122	8
2	1	4.6	0.66	20	2090	44 000	128	6
3	1	6.1	0.88	20	850	57 700	129	4
4	1	5.2	0.44	60	800	23 000	104	23
5	1	8.0	0.66	60	860	30 300	115	12
6	1	10.6	0.88	60	240	28 300	117	15
7	1	3.3	0.66	0	740	83 900	129	1
8	1	6.2	0.66	40	2420	37 400	120	7
9	2	1.5	0.22	20	1500	[i]	44	54
10	2	4.6	0.66	20	3080	[I]	86	31
11	2	6.1	0.88	20	2180	[I]	105	11

[a] [Ni] = 20 μmol l^{-1}, [Al] = 20 mmol l^{-1}.
[b] Pressure in the polymerization vessel.
[c] Ethylene concentration in toluene [14].
[d] Polymerization temperature.
[e] Activity, calculated from the mass of the polymer, catalyst concentration, monomer concentration and polymerization time.
[f] Molar mass determined by GPC against polyethylene standard.
[g] Determined by DSC (heating rate 20 K min^{-1}).
[h] Number of branching carbons per 1000 carbon atoms, determined by ^{1}H-NMR and ^{13}C-NMR spectroscopy.
[i] Samples only partially soluble due to high molecular weight (>10^7 g mol^{-1}).

branches. In agreement with those results, the catalytic activity was determined as a function of temperature, monomer concentration, and catalyst structure in some detail for the above catalysts. The polymerization results are summarized in Table 3 and can be interpreted by the reaction steps depicted in Scheme 2.

Fig. 4 shows the dependence of the catalytic activity on the concentration of ethylene in the polymerization solution. The catalytic activity varies depending on ethylene pressure and reaction temperature. At higher ethylene concentration the catalytic activity drops. By increasing the reaction temperature from 20 to 60°C the catalytic activity decreases. Nevertheless, at a reaction temperature of 60°C, a higher initial activity is observed, but fast deactivation of the catalyst causes loss of overall polymerization activity. At a reaction temperature of 20°C deactivation of the catalyst is slower and the overall polymerization activity is higher.

As seen in Fig. 5 there is a dependence of the number of branches/1000C (N) and polymer melting temperature (T_m) on reaction temperature. By increasing the reaction temperature more branches in the obtained polymer are observed. Because of the direct dependence

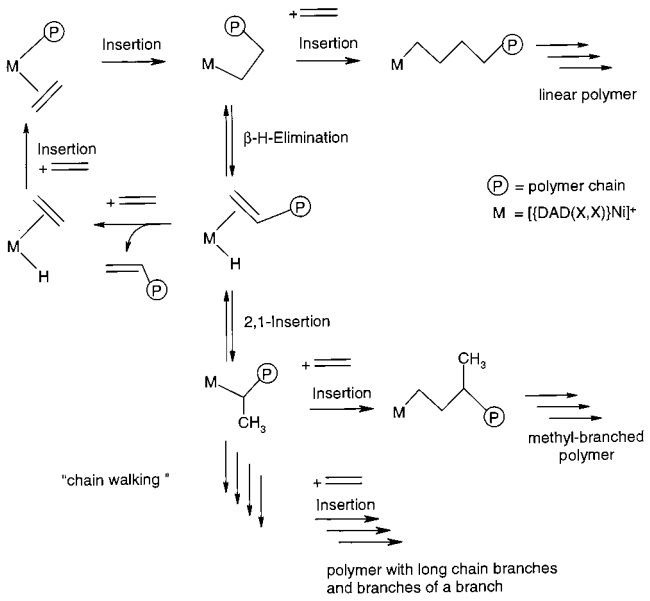

Scheme 2. Polymerization and branching mechanism.

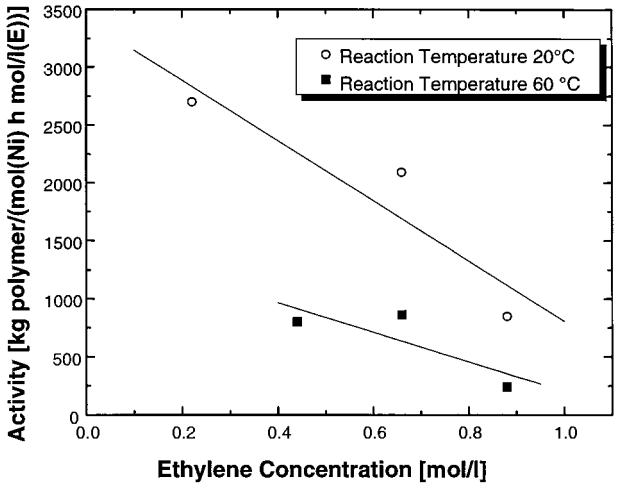

Fig. 4. Polymerization activity of **1**/MAO versus concentration of ethylene at different reaction temperatures.

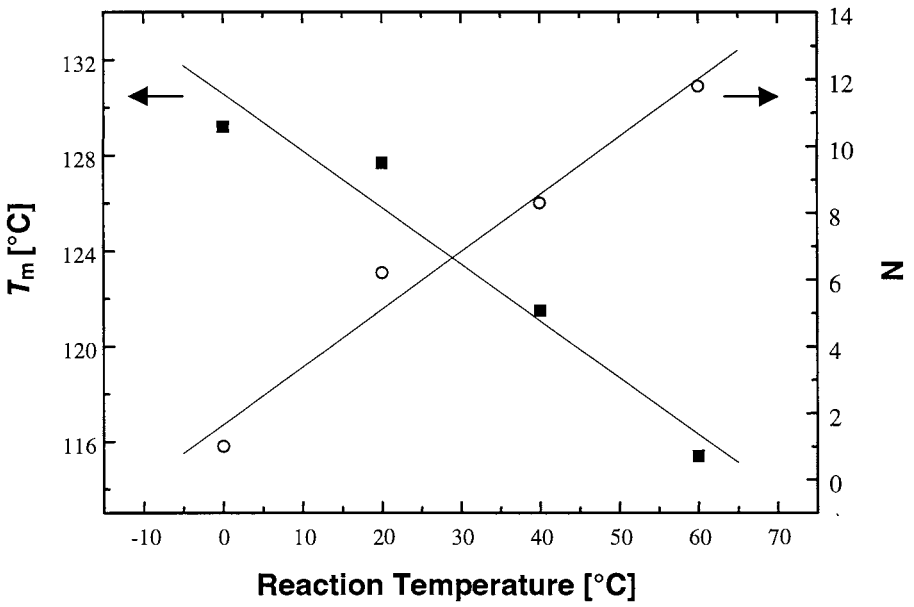

Fig. 5. Polymer melting temperature, T_m, and number of branches/1000C, N, of polyethylene obtained with **1**/MAO versus the reaction temperature (at a polyethylene concentration of 0.66 mol l^{-1}).

between the number of branches/1000C (N) and the polymer melting temperature, it is obvious that when the number of branches in the polymer rises the polymer melting temperature drops.

Fig. 6 shows the dependence of the polymer melting temperature (T_m) on the ethylene pressure. Decreasing the ethylene pressure leads to more branches in the polymer and so to a lower polymer melting temperature. This is the case for the catalytic systems derived from both **1** and **2**. The dependence of N and T_m on the ethylene pressure at different reaction temperatures is shown. At elevated reaction temperature more branches are formed and as a result the polymer melting temperature drops. The catalyst generated from **2** shows a stronger dependence of N and T_m on ethylene pressure than the analog generated from **1**.

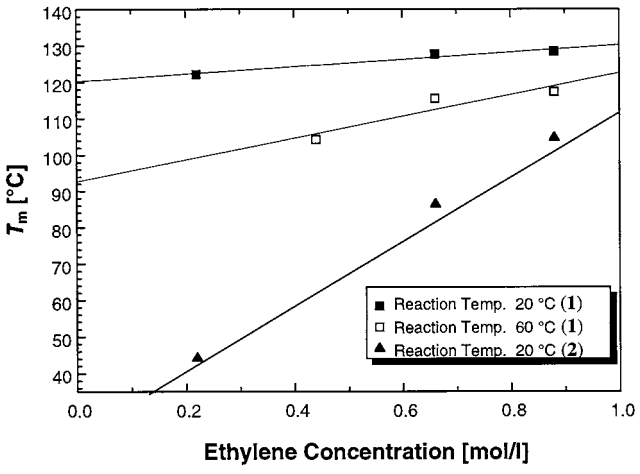

Fig. 6. Polymer melting temperature T_m versus the ethylene concentration obtained with **1**/MAO and **2**/MAO at different reaction temperatures.

The termination reaction appears to be more feasible for **1** than for **2**. The molecular weights of the polyethylenes generated with **2** are higher than those formed using **1**. This may suggest that the sterically more hindered nickel center of the catalytic species derived from **2** are longer-lived and may suppress termination by associative olefin exchange of the monomer. Provided that the insertion reaction of ethylene is the rate determining step [4,15,16], the significantly higher steric hindrance of the isopropyl groups of the catalyst formed from **2** compared to that of the catalyst formed from **1** may result in a more reactive, destabilized resting state. This is in line with the conformational differences of the {DAD(X,X)}Ni fragment found for the model compounds **3** and **4**.

In agreement with previous observations [4,12], the degree of branching N, determined by NMR spectroscopy as the number of methyl groups per 1000 carbon atoms, decreases with increasing ethylene pressure. The difference in ligand structure also influences the number of branches, *N*. This number is higher for all polymers produced by catalyst **2** compared to the polymers generated with **1** under the same polymerization conditions (see entry 1 and 9, 2 and 10). Branches are formed when β-hydride elimination of the growing polymer chain, followed by isomerization, occurs (Scheme 2). Isomerization is possible when the polymer chain at the nickel center undergoes β-hydride elimination forming an intermediate olefin hydride complex and the olefin reinserts in a 2,1-manner into the nickel–hydride bond before insertion of the next monomer

takes place. Somewhat counterintuitive, more isomerization and branching occurs if there is less space at the catalytic site. One would assume that the 2,1-insertion of the olefin should be sterically more hindered. Thus with the sterically more hindered, but more active catalyst precursor **2** higher branching frequencies are observed. In calculations [15,16], based on QM or combined QM/MM methods, where the nickel center with the attached ligands is calculated by quantum mechanics and the steric demanding groups are refined by molecular mechanics, a lower $\Delta G^{\ddagger}$ value was found for isomerization than for insertion. This leads to the conclusion that a more stable resting state of the catalyst allows more isomerization of the polymer chain to take place resulting in a higher degree of branching of the generated polymer.

3. Experimental

All operations were performed under an inert atmosphere of argon using standard Schlenk-line and glovebox techniques. Diethyl ether and hexane were dried over sodium/triglyme benzophenone ketyl and distilled under argon. DAD(H,H), DAD(Me,Me), {DAD-(H,H)}$NiBr_2$ (**1**), {DAD(Me,Me)}$NiBr_2$ (**2**) were prepared according to literature procedures [6]. Trimethylsilylmethyl magnesiumchloride was used as 1.0 M solution in diethyl ether (Aldrich). ^{1}H- and ^{13}C{H}-NMR spectra were recorded on a Bruker ARX200, ARX300, ARX400, and DRX400 spectrometer in benzene-d_6 at r.t. and in $C_2D_2Cl_4$ at 100°C for the polymers. Elemental analyses were determined on a Heraeus CHN-Rapid instrument. IR-spectra were recorded in concentrated dichloromethane solutions using a closed sample cell equipped with KBr windows on a Mattson Galaxy 2030 FT-IR spectrometer.

3.1. {DAD(H,H)}Ni(CH_2SiMe_3)$_2$ (3)

To a stirred suspension of {DAD(H,H)}$NiBr_2$ (555 mg, 0.93 mmol) in 20 ml of diethyl ether at −78°C was dropwise added a solution of trimethylsilylmethyl magnesiumchloride (1.86 ml of the 1 M solution in diethyl ether, 1.86 mmol). The color of the suspension changed to dark blue. After 1 h the suspension was allowed to warm to 0°C and stirring was continued for another hour. During this time, the color of the reaction mixture changed to green. All volatiles were removed in vacuo and the blue-green brittle foam was extracted at 0°C with 100 ml of cold hexane. The blue-green hexane extracts were filtered through celite to remove the magnesium halides, concentrated to 10 ml in vacuo, and cooled to −30°C to induce crystallization. After 2 days turquoise prisms (100 mg, 0.17 mmol) were obtained in 18% yield, suitable for a crystal structure analysis. ^{1}H-NMR (200 MHz): δ 0.08 (s, 18 H, $SiCH_3$), 0.88 (d, $^3J_{HH} = 6.8$ Hz, 6 H, $CH(CH_3)_2$), 1.52 (d, $^3J_{HH} = 6.8$ Hz, 6 H, $CH(CH_3)_2$), 2.32 (s, 4 H, CH_2SiMe_3), 3.56 (sept, $^3J_{HH} = 6$ 8 Hz, 4 H, $CH(CH_3)_2$) 7.35 (m, 6 H, C_6H_3), 9.07 (s, 2H, N=CH). ^{13}C{^{1}H}-NMR (100.6 MHz): δ −3.2 (CH_2SiMe_3), 3.4 ($SiCH_3$), 23.0, 25.3 ($CH(CH_3)_2$), 28.7 ($CHMe_2$), 124.1 (*meta*-C), 127.0 (*para*-C), 140.1 (*ortho*-C), 147.1 (*ipso*-C), 162.9 (N=CH); ^{29}Si{^{1}H}-NMR (79.5 MHz): δ 4.42. Anal. Calcd. for $C_{34}H_{58}N_2NiSi_2$: C 66.98, H 9.59, N 4.59. Found: C 66.93, H 9.73, N 7.91.

3.2. {DAD(Me,Me)}Ni(CH_2SiMe_3)$_2$ (4)

This compound was prepared following a similar procedure as described for **3** using {DAD(Me,-Me)}$NiBr_2$ (**2**) (640 mg, 1.0 mmol) and trimethylsilylmethyl magnesiumchloride (2 ml of 1 M solution in diethyl ether) to give 175 mg (0.28 mmol) of turquoise prisms, yield: 28%. ^{1}H-NMR (400 MHz): δ 0.05 (s, 6 H, N=CCH_3), 0.23 (s,18 H, SiCH_3), 0.93 (d, $^3J_{HH} = 6.8$ Hz, 6 H, $CH(CH_3)_2$), 1.17 (s, 4H, CH_2 $Si(CH_3)_3$), 1.53 (d, $^3J_{HH} = 6.8$ Hz, 6 H, $CH(CH_3)_2$), 3.58 (sept, $^3J_{HH} = 6.8$ Hz, 2 H, $CH(CH_3)_2$), 7.3 (m br, 6 H, C_6H_3); ^{13}C{^{1}H}-NMR (100.6 MHz): δ −5.6 (N=CCH_3), 4.1 ($SiCH_3$), 22.8 (CH_2SiMe_3), 24.2, 24.6 ($CH(CH_3)_2$), 28.6 ($CHMe_2$), 124.1 (*para*-C), 127.0 (*para*-C), 140.1 (*ortho*-C), 147.1 (*ipso*-C), 162.9 (N=CMe). Anal. Calcd. for $C_{36}H_{62}N_2NiSi_2$: C 67.80, H 9.80, N 4.05, Found: C 66.26, H 9.19, N 4.39.

3.3. {DAD(H,H)}Ni(CO)$_2$ (5)

A solution of {DAD(H,H)}Ni(CH_2SiMe_3)$_2$ (**3**) (71 mg, 0.1 mmol) in 50 ml of hexane was reacted with carbon monoxide in a 100 ml Schlenk flask by exchanging the argon atmosphere over the solution by carbon monoxide (1 bar) under stirring. The color of the solution changed immediately from blue green to red. After exchanging the atmosphere over the solution back to argon, the solution was concentrated to 5 ml and allowed to crystallize for 2 days at −30°C. Purple-red crystals suitable for crystal structure analysis were obtained in 43% yield. ^{1}H-NMR (200 MHz): δ 0.08 (s, 18 H, SiCH_3), 0.88 (d, $^3J_{HH} = 6.8$ Hz, 6 H, $CH(CH_3)_2$), 1.52 (d, $^3J_{HH} = 6.8$ Hz, 6 H, $CH(CH_3)_2$), 2.32 (s, 4 H, CH_2SiMe_3), 3.56 (sept, $^3J_{HH} = 6$ 8 Hz, 4 H, $CH(CH_3)_2$,) 7 35 (m, 6 H, C_6H_3), 9.07 (s, 2H, N=CH). ^{13}C{^{1}H}-NMR (100.6 MHz): δ 23.7, 25.5 ($CH(CH_3)_2$). 27.9 ($CHMe_2$), 123.7 (*meta*-C), 126.5 (*para*-C), 139.1 (*ortho*-C), 152.3 (*ipso*-C), 163.4 (N=CH), 196.9 (CO). IR (CH_2Cl_2): ν_{CO} (cm^{-1}): 2014, 1954.

The mother liquor was analyzed by NMR spectroscopy and contains ($Me_3SiCH_2)_2CO$ (**7**): ^{1}H-NMR (200 MHz): δ 0.21 (s, 9 H, SiCH_3), 2.22 (s, 2 H, CH_2SiMe_3). ^{13}C{^{1}H}-NMR (100.6 MHz): δ −1.2

Table 4
Crystallographic data for **3**, **4**, and **5**

Compound	**3**	**4**	**5**
Chemical formula	$C_{34}H_{58}N_2NiSi_2$	$C_{36}H_{62}N_2NiSi_2$	$C_{28}H_{36}N_2NiO_2$
Formula weight	609.71	637.77	491.30
Crystal size (mm)	$0.45\times0.5\times0.5$	$0.3\times0.4\times0.7$	$0.4\times0.4\times0.5$
Crystal system	Monoclinic	Monoclinic	Orthorhombic
Space group	$C2/c$ (No.15)	$C2/c$ (No.15)	$Pnma$ (No. 62)
Unit cell dimensions			
a (Å)	17.899(4)	10.503(3)	12.123(2)
b (Å)	10.343(2)	20.481 (2)	21.454(3)
c (Å)	20.197(3)	18.482(5)	10.614(4)
β (°)	98.57(1)	102.92(3)	
V (Å^3)	3697(1)	3875(2)	2761 (1)
Z	8/2	8/2	8/2
ρ_{calcd} (g cm^{-3})	1.095	1.093	1.182
μ (mm^{-1})	0.612	0.586	0.727
$F(000)$	1328	1392	1048
Temperature (K)	296(2)	296(2)	296(2)
2θmax [°]	56.0	58.0	60.0
Index ranges	$0\le h\le23$, $0\le k<13$, $-26\le l\le26$	$-10\le h\le14$, $-19\le k\le27$, $-25\le l\le24$	$0\le h\le17$, $0\le k\le30$, $0\le l\le14$
Absorption correction empirical (Ψ-scans)			
Transmission (min/max)	99.18/99.95	97.94/99.95	98.13/99.93
Reflections			
Collected/independent	4585/4449 ($R_{int}=0.0180$)	7149/5145 ($R_{int}=0.0132$)	4111/4111
Independent with $I>2\sigma(I)$	3613	3597	2450
No. of parameters	293	194	180
$R_1/wR_2/\sigma$; (all data)	0.0491/0.0974/1.070	0.0875/0.1351/1.041	0.1079/0.1209/1.142
$R_1/wR_2/\sigma$ [$I>2\sigma(I)$]	0.0316/0.0808/0.995	0.0468/0.1135/1.053	0.0455/0.0895/1.111
Resid. Electron density (e A^{-3})	0.268/−0.218	0.456/−0.283	0.435/−0.278

($SiCH_3$), 39.8 (CH_2SiMe_3), 147.9 (C=O). IR (CH_2Cl_2): ν (cm^{-1}): 2965, 1669 (C=O), 1256. Experiments on NMR-tube-scale in benzene-d_6 showed the presence of the second byproduct $Me_3SiCH_2CH_2SiMe_3$ (**6**), characterized by its resonances. ^{1}H-NMR (400 MHz): δ 0.08 (s, 18H, $SiCH_3$), 0.44 (s, 4H, CH_2) [17].

3.4. Polymerization procedure

The ethylene polymerization reactions using {DAD(H,H)}$NiBr_2$ (**1**) and {DAD(Me,Me)}$NiBr_2$ (**2**) precatalysts were performed in a mechanically stirred 1 l glass reactor. Typically, 400 ml of toluene was pumped into the reactor. After thermal equilibration of the reactor system ethylene was continuously added by a mass-flow meter (F-111 C, Bronkhorst, NI-7261 AK Ruurlo, Netherlands) until the reaction mixture was saturated with ethylene. The polymerization was started by adding 8 μmol of **1** or **2** in 8 ml of a 1:1 mixture of toluene and MAO solution, so that [Ni] = 20 μmol l^{-1} and [Al] = 20 mmol l^{-1}. The vapor pressure of the solvent was considered when calculating the ethylene concentration. Typically, polymerization was quenched by adding 10 ml isopropanol after 1 h. The polymer was precipitated in 1.5 l of methanol acidified with 10 ml of 10 wt.% hydrochloric acid, filtered, and dried at 60°C under vacuum.

3.5. Crystal strucure determination of {DAD(H,H)}-$Ni(CH_2SiMe_3)_2$ (3), {DAD(Me,Me)}$Ni(CH_2SiMe_3)_2$ (4) and {DAD(H,H)}$Ni(CO)_2$ (5)

{DAD(H,H)}$Ni(CH_2SiMe_3)_2$ (**3**) and {DAD(Me,-Me)}$Ni(CH_2SiMe_3)_2$ (**4**) were obtained as turquoise prisms by cooling concentrated hexane solutions of the compounds to −30°C. {DAD(H,H)}$Ni(CO)_2$ (**5**) was obtained as red prisms by cooling a concentrated hexane solution of the compound to −30°C. X-ray diffraction data were collected with an Enraf-Nonius CAD4 diffractometer at room temperature by using Mo–K_α radiation and ω-scans. Data reduction was carried out using the program system MolEN ([13]a). The structures were solved by direct methods (SHELXS-86) ([13]b) and refined by fullmatrix least squares (SHELXL-93) ([13]c) against F^2. Non-hydrogen atoms were refined anisotropically. For **3**, all hydrogen atoms were located in difference Fourier maps and refined in their position. Isotropic temperature

factors were also refined. For **5**, the hydrogen atoms not belonging to methyl groups were refined in their position; the other hydrogen atoms (as well as all hydrogen atoms in **4** were included in calculated positions with fixed thermal parameters. Crystallographic data are summarized in Table 4. Further details of the crystal structure determinations are available on request from the Fachinformationzentrum Karlsruhe, Gesellschaft für wissenschaftlich-technische Information mbH, D-76344 Eggenstein-Leopoldshafen, on quoting the depository number CSD-408809 (**3**), 408808 (**4**) and 408810 (**5**), the names of the authors, and the journal citation.

Acknowledgements

This research was supported by the German Federal Ministry for Education, Science, Research, and Technology (BMBF) (Project no. 03N10280) and the BASF AG as well as the Fonds der Chemischen Industrie. We thank Professor M. Brookhart for some discussion. WITCO GmbH, Berkamen, kindly supplied us with MAO solutions.

References

[1] (a) G. Wilke, Angew. Chem Int. Ed. Engl. 27 (1988) 185. (b) P.W. Jolly, G. Wilke, The Organic Chemistry of Nickel, vol. 1, Academic Press, New York, 1975. (c) Wilke, G.; Herrmann, G. Angew. Chem. 1966, 78, 591.

[2] (a) W. Keim, R. Appel, A. Storeck, C. Kruger, R. Goddard, Angew. Chem. 93 (1981) 91. (b) M. Peuckert, W. Keim, Organometallics 2 (1983) 594. (c) For a recent review on oligomerization of ethylene see, D. Vogt in Applied Homogeneous Catalysis with Organometallic Compounds (Eds.: B. Cornils, W.A. Herrmann), vol.1, chapter 2.3.1.3, VCH Verlagsgesellschaft, Weinheim, 1996. (d) U. Klabunde, S.D. Ittel, J. Mol. Cat. 41 (1987)123. (e) K.A. Ostaja Starzewski, J. Witte, Angew. Chem. 97 (1985) 610. (f) K.A. Ostaje Starzewski, J. Witte, Angew. Chem. 99 (1987) 76.

[3] G. Fink, V.M. Mohring, Angew. Chem Int. Ed. Engl. 24 (1985) 1001.

[4] (a) L.K. Johnson, C.M. Killian, M. Brookhart, J. Am. Chem. Soc. 117 (1995) 6414. (b) L.K. Johnson, S. Mecking, M. Brookhart, J. Am. Chem. Soc. 118 (1996) 267. (c) M. Brookhart, L.K. Johnson, C.M. Killian, S. Mecking, D.J. Tempel, Polymer Preprints 37 (2) (1996) 254. (d) Brookhart/DuPont Pat. Appl. WO 96/23010. (e) C.M. Killian, L.K. Johnson, M. Brookhart, Organometallics 16 (1997) 2005. (e) S. Mecking, L.K. Johnson, L. Wang, M. Brookhart, J. Am. Chem. Soc. 120 (1998) 888.

[5] For a review on 1,4-diazadiene complexes, see (a) G. van Koten, K. Vrieze, Adv. Organomet. Chem. 21 (1982) 151, and references therein. (b) J.H. Groen, C.J. Elsevier, K. Vrieze, W.J.J. Smeets, A.L. Spek, Organometallics 15 (1996) 3445. (c) H.F. Haarman, F.R. Bregman, J.M. Ernsting, N. Veldman, L.A. Spek, K. Vrieze, Organometallics 16 (1997) 54.

[6] (a) H. tom Dieck, M. Svoboda, Chem. Ber. 109 (1976) 1657. (b) M. Svoboda, Ph. D. Thesis 1978, University of Frankfurt, Main, Germany. (c) M. Svoboda, H. tom Dieck, Organomet. Chem. 191 (1980) 321.

[7] (a) H. tom Dieck, M. Svoboda, T.Z. Greiser, Naturforsch. 36B (1981) 823. (b) M. Svoboda, H. tom Dieck, C. Kruger, Y.H. Tsay, Z. Naturforsch. B 36B (1981) 814. (c) H. tom Dieck, M. Svoboda, J. Kopf, Z. Naturforsch. 33B (1978) 1381.

[8] J. Okuda, F.J. Schattenmann, S. Wocadlo, W. Massa, Organometallics 14 (1995) 789.

[9] (a) T. Yamamoto, T. Kohara, A. Yamamoto, Chem. Lett. (1976) 1217. (b) T. Kohara, S. Komiya, T. Yamamoto, A. Yamamoto, Chem. Lett. (1979) 1513. (c) S. Komiya, Y. Abe, A. Yamamoto, T. Yamamoto, Organometallics 2 (1983) 1466. (d) K. Tatsumi, A Nakamura, S. Komiya, A. Yamamoto, T. Yamamoto, J. Am. Chem. Soc. 106 (1984) 8181.

[10] E. Carmona, F. Gonzalez, M.L. Poveda, J.L. Atwood, R.D. Rogers, J. Chem. Soc. Dalton Trans. (1981) 777.

[11] (a) G. Sonnek, E. Dinjus, Z. Anorg. Allg. Chem. 441 (1978) 58. (b) J. Sieler, R. Benedix, N.N. Than, E. Dinjus, D. Walther, Z. Anorg. Allg. Chem. 522 (1985) 131.

[12] (a) R.F. de Souza, R.S. Mauler, L.C. Simon, F.F. Nunes, D.V.S. Vescia, A. Cavagnolli, Macromol. Rapid. Commun. 18 (1997) 795. (b) D. Pappalardo, M. Mazzeo, C. Pellecchia, Macromol. Rapid. Commun. 18 (1997) 1017.

[13] (a) C.K. Fair, MolEN, An Interactive Structure Solution Procedure; Enraf-Nonius, Delft, The Netherlands, 1990. (b) G.M. Sheldrick, SHELXS-86, Program for the Solution of Crystal Structures; University of Göttingen, Göttingen, Germany, 1986. (c) G.M. Sheldrick, SHELXL-93, Program for the Refinement of Crystal Structures, University of Göttingen, Göttingen, Germany, 1993.

[14] W. Krauss, W. Gestrich, Chem. Tech. 6 (1977) 513.

[15] (a) L. Deng, P.M. Margl, T. Ziegler, J. Am. Chem. Soc. 119 (1997) 1094. (b) L. Deng, T.K. Woo, L. Cavallo, P.M. Margl, T. Ziegler, J. Am. Chem. Soc. 119 (1997) 6177.

[16] (a) D.G. Musaev, R.D.J. Froese, M. Svensson, K. Morokuma, J. Am. Chem. Soc. 119 (1997) 364. (b) D.G. Musaev, M. Svensson, K. Morokuma, S. Stromberg, K. Zetterberg, P.E.M. Siegbahn, Organometallics 16 (1997) 1933. (c) R.D.J. Froese, D.G. Musaev, K. Morokuma, J. Am. Chem. Soc. 120 (1998) 1581.

[17] (a) I. Fleming, A. Pearce, J. Chem. Soc. Perkin (1981) 251. (b) D. Djahanbini, B. Cazes, J. Gore, F. Gobert, Tetrahedron 41 (1985) 867.